Structural and Spectral Studies of Halogen Bonding and Anion-Pi Interactions with Halide and Pseudohalide Anions

An Honors Thesis (HONR 499)

by

Olivia A. Grounds

Thesis Advisor

Sergiy Rosokha

Ball State University

Muncie, Indiana

November 2018

Expected Date of Graduation

May 2019

Abstract

Halogen and anion-π bondings represent unexpected types of intermolecular interactions which attracted the attention of chemists over the last two decades. Halogen bonding is an attraction of electron-rich species to halogen atoms. It is similar to the well-known hydrogen bonding, and the differences between hydrogen and halogen bonds have been hard to distinguish. Using UV-Vis and ^{1}HNMR measurements in solutions and X-ray crystallography in the solid-state, we were able to determine when each bond was likely to form and the different characteristics that each bond showed. In particular, it was found that the formation of halogen bonds leads to the appearance of new and intense peaks in the absorption bands in the UV-Vis spectra while hydrogen bonds would merely result in some shift of the less intense absorption bands or reagents. Also, halogen bonds and anion-π interactions are most commonly explained as an attraction of electron-rich (negative) species to the areas of positive charge (referred to as σ- and π-holes) which sometimes exists on the surfaces of halogens and π-molecules. However, in the current work we demonstrated and clarified exceptions to this model. Specifically, X-ray structural analysis showed that arrangements of many anion-π and halogen-bonded reactants deviate substantially from the location of the most positive or negative potentials on their surfaces. Instead, they follow locations of the frontier orbitals of interacting species. This suggests that frontier-orbital interactions represent the major factor determining the structures of these intermolecular complexes.

Acknowledgments

This research was started in the fall of 2016, during which time it was funded by the National Science Foundation (grant CHE1607746).

Also, a special thanks to my mentor on this project, Dr. Sergiy Rosokha, for allowing me to work on such an interesting topic. He made such a large undertaking much easier through his guidance.

I would also like to thank everyone in my lab group for being a part of this experience, especially Brandon Watson for working as my partner on these projects and helping me collect data.

Lastly, I would like to thank Dr. Matthias Zeller at Purdue for X-ray structural analysis for all the crystals I prepared.

Table of Contents

1. Watson, B.; Grounds, O.; Borley, W. Rosokha, S.V.;* Resolving Halogen vs Hydrogen Bonding Dichotomy in Solutions: Intermolecular Complexes of Trihalomethanes with Halide and Pseudohalide Anions. *Physical Chemistry Chemical Physics*, **2018**, *20,* 21999-22007.
2. Grounds, O.; Zeller, M.; Rosokha, S.V.;* Structural preferences in strong anion-π and halogen-bonded complexes: π- and σ-holes vs frontier orbitals interaction. *New Journal of Chemistry,* **2018**, *42*, 10572-10583.

Process Analysis Statement

I started researching with Dr. Sergiy Rosokha in October 2016 as an intern in his laboratory at Ball State University. Dr. Rosokha studies intermolecular interactions and how they affect reactions; he is a foremost expert on halogen bonding and anion-π interactions, which are my research topic.

I studied halogen bonds between halide or pseudohalide anions in conjunction with a trihalomethane, iodoform in solution as well as in their crystalline form. I would take UV-Vis spectra of these complexes in acetonitrile to find their equilibrium constant and absorptivity. I also prepared crystals of these complexes through solvent diffusion to find the type of bonds created and the bond lengths using x-ray crystallography. Using this information, I then compared it to information on hydrogen bonds to find a way to distinguish the two types of interactions and predict which types of bonds would form with certain compounds.

Also, I studied anion- π interactions and the deviations of halogen-bonded and anion-π complexes from the electrostatic model that dictates the typical contacts between the electron donor and acceptor. Through previous research, Dr. Rosokha noticed that there were exceptions to the model, so we prepared crystals through solvent diffusion and slow evaporation of solvents. After obtaining our structures using x-ray crystallography, we compared the experimental data with Dr. Rosokha's computational data to find reasons for such deviations.

This research is just a start into these fields. The electrostatic model is an imprecise model and there is a chance that it might not be what truly governs the placement of these contacts. Also, both halogen bonds and anion- π interactions have

many possible future uses, such as in medicine and crystal engineering. These fields are relatively new and ever evolving; more data is collected every day that gives a better insight into what makes up these bonds and other possible ways that this can be used in the future.

Experimental results obtained in this work allowed us to clarify properties and structural preferences of halogen and anion-π bonding and they are published in two articles in peer-reviewed scientific journals:

3. Watson, B.; Grounds, O.; Borley, W.; Rosokha, S.V.;* Resolving halogen vs hydrogen bonding dichotomy in solutions: Intermolecular complexes of trihalomethanes with halide and pseudohalide anions. *Physical Chemistry Chemical Physics*, 2018, *20,* 21999 - 22007. (Watson, B. and Borley, W. are BSU students, Brandon did NMR measurements, and William did computations).

4. Grounds, O.; Zeller, M.; Rosokha, S.V.;* Structural preferences in strong anion-π and halogen-bonded complexes: π- and σ-holes vs frontier orbitals interaction. *New Journal of Chemistry,* 2018, *42*, 10572-10583. (M. Zeller from Purdue University did X-ray structural analysis of the crystals).

These publications are attached as Supplemental Materials.

The results of work were presented at several conferences (presenter is listed first):

1. Watson, B., Grounds, O., and Rosokha, S. V. Halogen to hydrogen bonding switch in complexes of iodo-, bromo-, and chloroform with anionic and neutral nucleophiles. American Chemical Society. 255th Annual National Meeting of the American Chemical Society, New Orleans, LA, March 18-22, 2018. (Oral presentation).

2. Grounds, O., Watson, B., Borley, W., Rosokha, S. V. Characterization of Halogen and Hydrogen-Bonded Complexes of Iodoform and Bromoform with (Pseudo-) Halide Anions. 3rd International Symposium for Halogen Bonding. ISXB-3. Greenville, SC, June 12, 2018. (Poster presentation).

3. Grounds, O., Rosokha, S. V. Unusual structural features of halogen bonded and anion π complexes, 255th Annual National Meeting of the American Chemical Society, New Orleans, LA, March 18-22, 2018. (Poster presentation).

4. Grounds, O.; Watson, B.; Rosokha, S.V. Halogen bonding of iodoform with neutral and anionic nucleophiles. Book of Abstracts. 48th Central Regional Meeting of the American Chemical Society. June 6-10, 2017, Dearborn, MI, p. 79 (Poster presentation).

Introduction

Halogen and anion-π bonding are very unusual intermolecular interactions which attracted attention of scientists during the last 15 – 20 years. Halogen bonding (XB) is an intermolecular attraction of an electron poor (electrophilic) halogen atom to an electron-rich species (nucleophiles).[1] This bonding is illustrated in Figure 1 (left) in which an X (where X = Br, Cl, I, or F) is a halogen, D is typically a carbon or nitrogen which is bonded to X (D-X is a XB donor), and an electron-rich anion is shown as a red sphere.

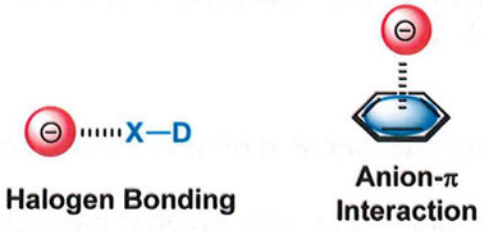

Figure 1. The left image shows an interpterion of halogen bonding. It shows the attraction between the nucleophile and the halogen as well as the bond to the carbon or nitrogen (D). The right image shows an example for an anion-π interaction.

Halogen bonds are an extremely unique and complicated system. These bonds could be found in the substances prepared in 1814, (although they were not recognized as halogen bonds at that time).[1] In the 1950s, the coupling of Robert Mulliken's discovery of electron acceptor/donor relationships and Odd Hassel's work with crystallography established halogen-bonded complexes in solid-state and in solutions. Along the way, many possible theories were placed forth about why di- and tri-halides were able to interact with different anions and why the strength of the interactions were found dependent on which halogens are involved, with the general trend of these interactions being F < Cl < Br < I. Even after the work of Mulliken and Hassel came out, the research behind halogen bonding was varied and scattered. The study of halogen

bonds began to pick up steam in the late 1980s and since then many features and uses have been found. The recent publications commonly relate halogen bonding to attraction of electron-rich species (shown as red) to area of positive potential (so called σ-hole) on the surface of halogen atom (shown as blue in Figure 2).[2]

Figure 2. The blue on the left molecule shows the σ-hole while the red molecule indicates an electron rich molecule.

Anion-π interactions are a newer field of research that studies the non-covalent interactions between π-acceptors and anions. Anion-π interactions are an attraction of negatively charged species (anions) to molecules with π-bonds.[3] It is illustrated in Figure 1 (right). The first documented calculations to prove that anion-π bonding existed were done in 2002.[3] In 2004, the lab of Jay Kochi reported the first crystal that had anion-π interactions in it.[4] Anion-π interactions are not like most other bonds because they have a directionality to them, much like halogen bonds. Similar to halogen bonding, it is explained as an attraction of electron-rich species to the areas of positive potentials π-holes) on the surfaces of aromatic or olephinic molecules.[5]

Anthony Legon discovered the similarities between halogen bonds and well-known hydrogen bonds (HB).[6] Due to similarities between halogens and hydrogens as well as the fact that many molecules may form bonds with both of these, it is very difficult to distinguish them. So, the first goal of this work was to find out differences between these types of bondings and the factors which determine preferences of one

bond over the other. To explore XB/HB competition of the same molecule, we looked at the interaction of trihalomethanes, CHX_3 (X = I, Br, Cl) with (pseudo-)halide anions, A^- (A^- = Cl^-, Br^-, I^-, NCS^-, NCO^-, N_3^-). The CHX_3 molecules (shown in Figure 3) have both hydrogen and halogen substituents. Thus, they are the simplest species capable of both interactions, and they seemed well-suited to study competition and differences between HB and XB.

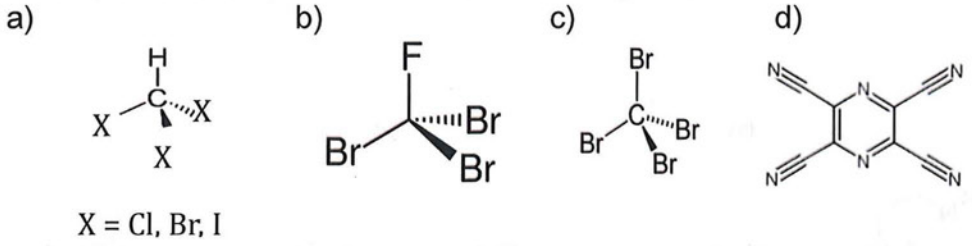

Figure 3. a) CHI_3 molecule, b) CBr_3F molecule, c) CBr_4 molecule, d) TCP molecule

Also, although halogen bonding and anion-π interactions were commonly assigned to electrostatic attraction (Figure 2), the significant deviations from the locations of positive and negative areas were observed earlier in many systems.[7,8] After determining this, it was decided that the second goal of this work was to check when and why these deviations occurred. To achieve this, we studied halogen bonding between CBr_4 and CBr_3F (Figure 3) with pseudohalide anions NCS^-, NCO^-, N_3^- as well as anion-π interaction of aromatic electron acceptor TCP (Figure 3) with halide anions (Cl^-, Br^-, I^-).

Experimental

2.1 Preparation of reactants. Electron-acceptors used in this study (Figure 3) are commercially available. To study halogen-bonding and anion-π interaction, we needed salts of halide and pseudohalide anions, so we had to prepare their salts with bulky counter-ions which are soluble in organic solvents. The structure and designations of these counter-ions are illustrated in Figure 4. These salts were prepared or purified as follows.

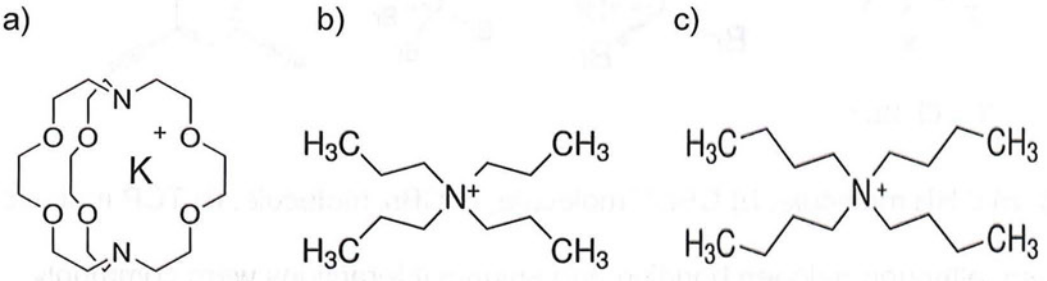

Figure 4. a) K(crp) counter-ion, b) TPA counter-ion, c) TBA counter-ion.

TPANCS. Approximately 3g of $TPABF_4$ was added to 40mL of methanol while there was low heating and stirring. Then, approximately 1.25g of KNCS was added to 15mL of methanol while there was low heating and stirring. The KNCS solution was added dropwise to the $TPABF_4$ solution over the course of 15 minutes. This was left to stir for 2 hours and then the precipitate was filtered off. The methanol was rotovaped off until there was 2-5mL of it left. Then, excess ethyl acetate was added to the flask (if it did not precipitate, rotovaped the ethyl acetate off and add it again). The solid was then filtered and weighed. The purity was checked using UV. If it was impure, a purification was done.

$TPAN_3$. This procedure was similar to the TPANCS synthesis. Approximately 3g of $TPABF_4$ was added to 40mL of methanol and about 1g of KN_3 was dissolved in 75mL of methanol. The rest of the procedure was the same.

TPANCO. This procedure was similar to the TPANCS synthesis. Approximately 4g of $TPABF_4$ was added to 50mL of methanol and about 1.24g of KNCO was added to 90mL of methanol. The rest of the procedure was the same.

K(crp)N_3. Approximately 0.75g of Kryptofix and 0.16g of KN_3 was added to 10mL of methanol. It was stirred for over an hour and then the solvent was rotovaped off. 25mL of DCM was added and the excess KN_3 was filtered off. The solution was rotovaped off until there was only 2-5mL of it left. Hexane was added until it precipitated. If it did not precipitate after 30mL of hexane, approximately 15mL of ethyl acetate was added. If it still did not precipitate, then the solvents were rotovaped off until about 2-5mL was left and ethyl acetate was added. It was then filtered and weighed. The purity was checked using UV. If it was impure, a purification of the salt was done.

K(crp)NCO. Approximately 0.15g of Kryptofix and 0.06g of KN_3 was added to 10mL methanol. The rest of the procedure was the same as the K(crp)N_3 synthesis.

K(crp)I. Approximately 0.15g of Kryptofix and 0.1g of KN_3 were added to 20mL of methanol. The rest of the procedure was the same as the K(crp)N_3 synthesis.

TPACl and TPABr purification. The salt was added to warm dichloromethane and then excess ethyl acetate was added to precipitate the salt out of the solution. Then, the salt was vacuum filtered off and inspected using UV to check for impurities.

Preparation of crystals for X-ray structural analysis.

Crystals comprised of CHI_3 combined with TBAI, TPACl, or TPABr were formed. The TPACl and TPABr crystals were produced by previous students, so the method was unclear while the TBAI crystals were synthesized during the project. This was done by taking 21.2mg TBAI and 23.1mg of CHI_3. These were added to 3mL of DCM and added into a test tube. Then a 3:1 DCM and hexane layer of 3mL was added on top of the bottom layer. A 1:1 layer of DCM and hexane of 3mL was added on top of the previous layer followed by 6mL of hexane on top of that. The mixtures were placed in a freezer and left to sit for a few days. Bond lengths between resulting halogen crystals were calculated and compared to known van der Waal radii.

Crystals comprised of TCP (tetracyanopyrazine) combined with TBABr, TPACl, K(crp)Br, or K(crp)Cl were prepared. They were diffused in an hexane:dichloromethane solution using a 1:1 molar ratio of the acceptor and halide salt at 0°C.

Crystals made up of TCP and K(crp)I were created using a slow evaporation of acetonitrile solutions which contained both compounds at 0°C.

Crystals which were comprised of CBr_4 and K(crp)NCS and crystals that were made of CBr_3F and TPANCS were created by the evaporation of solutions containing the pseudohalide salt and brominated electrophile in a 10:1 dichloromethane:hexane solution at room temperature.

2.2 UV-Vis measurements.

For all the complex combinations, a standard pattern was formed. To begin, approximately 50mg of the halide salt were added to 1mL of acetonitrile and then added to a 2mm cuvette. A spectrum was taken and examined for any absorption bands. If

there were none, then an experiment was performed. The halide salt was measured out to make an approximate 0.5M solution in 5mL of acetonitrile (AN) while approximately 22mg of CHI_3 was weighed out and added to 5mL of AN. 2mL of that solution was then taken and added to 8mL more of AN for a serial dilution, giving the solution an approximate 0.002 molarity. Then, a series of dilutions occurred to test how the concentration affected the absorption band.

Trial	1	2	3	4	5	6	7	8	9	10	11
X	0	0.5	0.5	0.3	0.2	0.15	0.1	0.07	0.04	0.02	0
CHI_3	0.5	0	0.5	0.5	0.5	0.5	0.5	0.5	0.5	0.5	0.5
AN	0.5	0.5	0	0.2	0.3	0.35	0.4	0.43	0.46	0.48	0.5

Table 1: The different volumes of each solution used during the different trials.

[HI_2C-I···Br TBA]

Two trials of [HI_2C-I···Br TBA] were run using a 2mm cuvette. TBA-Br solutions were individually prepared and dissolved in 5mL AN with 1207.8 mg (0.749M) and 1205.0mg (0.748M). The amount of CHI_3 added in 5mL of AN was, respectively, 20.5mg and 22.9mg. A serial dilution occurred by taking 2mL of the prepared CHI_3 and diluting it using 8mL more of AN. The respective concentrations of those solutions were 0.0020M and 0.0022M.

[HI_2C-I···Br TPA]

Two trials of [HI_2C-I···Br TPA] were run using a 2mm cuvette. TPA-Br solutions were individually prepared and dissolved in 5mL AN with 713.8 mg (0.536M) and 715.3mg (0.537M). The amount of CHI_3 added in 5mL of AN was, respectively, 22.3mg and 22.9mg. A serial dilution occurred by taking 2mL of the prepared CHI_3 and diluting it

using 8mL more of AN. The respective concentrations of those solutions were 0.0023M and 0.0023M.

[HI_2C-I ···Cl TBA]

Three trials of [HI_2C-I ··· Cl TBA] were run using a 2mm cuvette. TBACl solutions were individually prepared and dissolved in 5mL AN with 721.4mg (0.519M), 710.0mg (0.511M), and 716.8mg (0.516M). The amount of CHI_3 added in 5mL of AN was, respectively, 28.5mg, 21.1mg, and 23.6mg. A serial dilution occurred by taking 2mL of the prepared CHI_3 and diluting it using 8mL more of AN. The respective concentrations of those solutions were 0.0029M, 0.0021M, and 0.0024M.

[HI_2C-I ···NCS TPA]

Three trials of [HI_2C-I ··· NCS TPA] were run using a 2mm cuvette. TPANCS solutions were individually prepared and dissolved in 5mL AN with 300.6mg (0.246M), 508.1mg (0.416M), and 516.7mg (0.423M). The amount of CHI_3 added in 5mL of AN was, respectively, 21.0mg, 21.1mg, and 20.1mg. A serial dilution occurred by taking 2mL of the prepared CHI_3 and diluting it using 8mL more of AN. The respective concentrations of those solutions were 0.0021M, 0.0021M, and 0.0020M.

[HI_2C-I ···I TBA]

One trial of [HI_2C-I ···I TBA] was run using a 2mm cuvette. A TBAI solution was prepared and dissolved in 5mL AN with 313.3mg (0.488M). The amount of CHI_3 added in 5mL of AN was 21.8. A serial dilution occurred by taking 2mL of the prepared CHI_3 and diluting it using 8mL more of AN, creating a 0.0022M solution.

[HI_2C-I ···DABCO]

Four trials of [HI_2C-I $\cdots$ DABCO] were run using a 2mm cuvette. DABCO solutions were individually prepared and dissolved in 5mL AN with 318.7mg (0.568M), 349.3mg (0.623M), 313.2mg (0.558M), and 305.3mg (0.545M). The amount of CHI_3 added in 5mL of AN was, respectively, 19.9mg, 20.2mg, 19.6mg, and 19.7mg. A serial dilution occurred by taking 2mL of the prepared CHI_3 and diluting it using 8mL more of AN. The respective concentrations of those solutions were 0.0020M, 0.0021M, 0.0020M, and 0.0020M.

[HI_2C-I $\cdots$N-TPAN_2]

One trial of [HI_2C-I $\cdots$N-TBAN_2] was run using a 2mm cuvette. A TBAN_3 solution was prepared and dissolved in 5mL AN with 743.3mg (0.523M). The amount of CHI_3 added in 5mL of AN was 19.3mg. A serial dilution occurred by taking 2mL of the prepared CHI_3 and diluting it using 8mL more of AN, creating a 0.0020M solution.

Results and Discussion

3.1 Halogen vs. Hydrogen Bonding of CHI_3 with anions

There have been questions on why some halogenated complexes form only halogen bonds, only hydrogen bonds, or both. By using X-ray crystal structure on CHI_3, it was determined that the CHI_3 molecules favored halogen bonds over hydrogen. While looking at the bond lengths for CHI_3 crystals, it was noted that the distances between halogen atoms were shorter than the sums of the van der Waal radii of interacting atoms, which ranged anywhere from 10.4% to 16.4%. It was determined that when halogen bonds occur, these contractions would be seen.

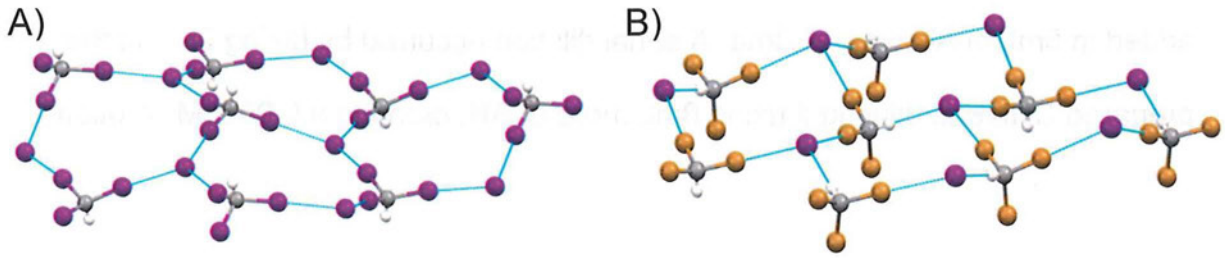

Figure 5: A) *[HI_2C-I $\cdots I^-$]* crystal. B) *[HBr_2C-Br $\cdots I^-$] crystal.* Blue lines show halogen and hydrogen bonds.

Yet, that is not the case for all trihalomethanes. In fact, $CHBr_3$ was found to take part in both types of bonding, however, it preferred hydrogen bonding over halogen, as seen in Figure 5. $CHCl_3$ was found to only like to except hydrogen bonds. Because we knew these preferences from x-ray crystallography, a few other things could be concluded.

When looking at these in solution, we came to a few interesting conclusions. During ^{1}HNMR tests done by Brandon Watson, it was noted that the hydrogen's position was shifting upfield or downfield depending on what was being run. It would shift upfield when CHI_3 was being tested, but it would shift downfield when $CHBr_3$ and $CHCl_3$ were

run. It was determined that the cause of this was the type of bonding it preferred. $CHBr_3$ and $CHCl_3$ have hydrogen bonds and these bonds cause a downfield shift due to the fact that the hydrogens become more deshielded when they are bonded to highly electronegative atoms.

Another way to determine whether or not a complex has halogen bonds is to take a UV-Vis spectra of them in solution. Halogen bonds will create new peaks in a spectra while hydrogen bonds do not. CHI_3 was characterized by absorption bands with peaks at 336nm, 296nm, and 265nm (Figure 6). The nucleophiles (halide anions with counter-ions) that were combined with the CHI_3 do not absorb in this spectral range. When there was an increase of any of these nucleophiles in the solution of CHI_3, there was an increase in the intensity of the absorption in this area and an eventual appearance of new absorption maxima (Figures 6 and 7).

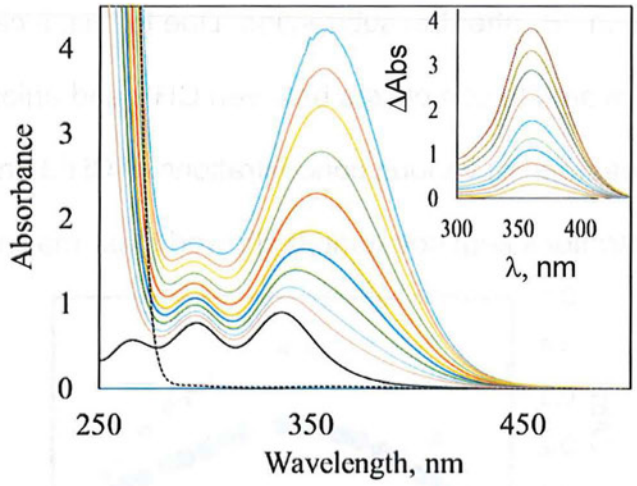

Figure 6. CHI_3 (4.6 mM) and various concentrations of TPAI (0, 4.6, 7.4, 12.4, 18.6, 24.8, 37.2, 54.6, 76.5, 98.3 and 131 mM, solid lines in descending order). Dashed line shows spectrum of the separate 200 mM solution of TPAI. Insert: Spectra of halogen-bonded complexes obtained by a subtraction of absorption of components from the spectra of solutions.

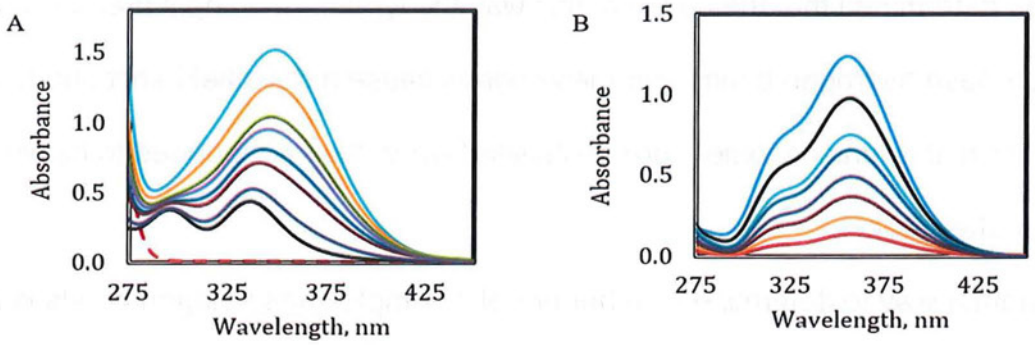

Figure 7: A) UV-Vis spectra of solutions containing N_3^- and CHI_3. B) Spectra of halogen-bonded complexes obtained by subtraction of absorption of components.

For all the UV- spectra taken for these systems, it appeared that there was an absorbance peak that formed which increased when the concentration of the halide salt was increased. However, it was not until after the subtraction that this band could be seen clearly. For the subtraction in each of the spectra, the peaks for CHI_3 and the halide salt were subtracted out of the different concentration peaks. For CHI_3 peaks, it was noted that the peaks were redshifted which is seen in Figure 7. The peaks go from 330nm in 7A) to 355nm in 7B) after the subtraction. Due to this, it can be assumed that the new bands can be related to complexes between CHI_3 and anions. The absorbance of the solutions was measured at various concentrations of CHI3 and anions ratios, but with the sum of concentrations kept constant. It showed clear maximum at 1:1 ratio (Figure 8).

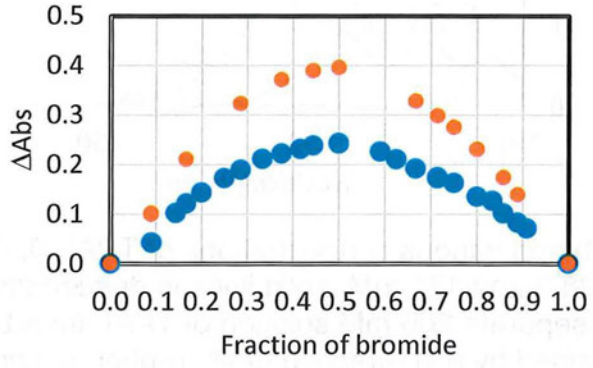

Figure 8. Job's plot to determine the change in absorbance on the molar fraction of bromide for the solution containing CHI_3 and Br^- with constant sum of the Blue points show absorption measured at λ= 340 nm while orange points are at λ= 296 nm.

This indicated that 1:1 complex is formed (eq 1).

$$CHI_3 + A^- \leftrightarrow [CHI_3, A^-] \quad (1)$$

Using the CHI_3 UV-Vis data, the equilibrium constant, which characterize strengths of the complex, and its absorptivity (ε values) were calculated. The formation constant of the complex is expressed as

$$K = \frac{[CHI_3,A^-]}{([CHI_3]-[CHI_3,A^-])([A^-]-[CHI_3,A^-])} \quad (2)$$

where $[CHI_3, A^-]$ is the concentration of the complex, and $[CHI_3]$ and $[A^-]$ are initial concentrations of CHX_3 and A^-, respectively. When $[A^-] >> [CHI_3]$, $[A^-] - [CHI_3] \approx [A^-]$. So, that means that

$K = \frac{[CHI_3,A^-]}{([CHI_3]-[CHI_3,A^-])([A^-])}$. Thus,

$$K([CHI_3] - [CHI_3, A^-])\,[A^-] - [CHI_3, A^-] = 0 \quad (3)$$

Or

$$[CHI_3, A^-] = K[CHI_3][A^-] \,/\, (K[CHI_3] + 1) \quad (4)$$

When $\Delta Abs = \varepsilon\, l\, [CHI_3, A^-]$, where ΔAbs is the absorbance of the complex at certain wavelength found after a subtraction, and l is the cell length, the latter can be rearranged as the Benesi-Hildebrand equation:

$$[CHI_3]/\Delta Abs = 1/(\varepsilon\, l) + \{1/(\varepsilon l\, K)\} \times 1/[A^-] \quad (5)$$

This gives $1/\varepsilon$ with a slope of $1/\varepsilon K$, so ε and K can be calculated. The examples of such dependence are shown in Figure 9.

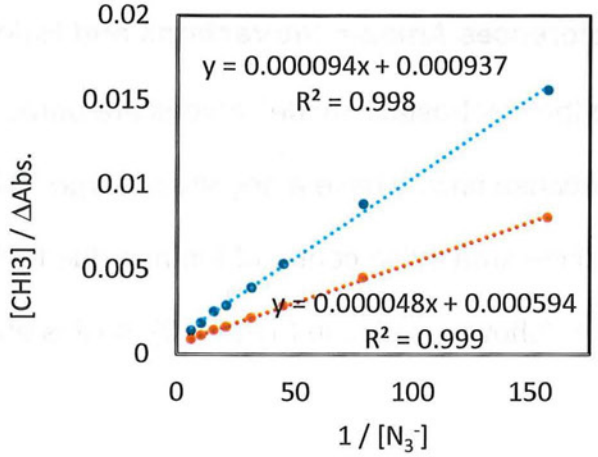

Figure 9. Benesi-Hildebrand equation done on CHI_3 with a N_3^- anion in an acetonitrile solution.

Formation constants K, absorption band maxima λ and absorptivity of the complexes obtained from these graphs are listed in Table 2.

Table 2. Formation constants of and extinction coefficients of [CHI_3, A^-] complexes.

CHX_3	A^{-b}	K_{UV}^{eff}, M^{-1}	λ , nm	ε, $M^{-1}cm^{-1}$
CHI_3	I^-	10.5±0.9	354±9	2729±564
	Br^-	11.7±1.0	341±2	1151±314
	Cl^-	9.2±0.6	333	1120±109
	NCS^-	2.4±0.5	346±1	1573±589
	NCO^-	9.2±2.1	321±4	539±621
	N_3^-	10.7±1.3	355	1167±252

Comparison of this data with the results of NMR measurements (done by Brandon Watson) and X-ray analysis allowed us to conclude that it is halogen bonded complexes which produced these bands. Thus, this data showed that CHI_3 prefers halogen bonding. Further computational analysis and comparison with the data for $CHBr_3$ and $CHCl_3$ (which was done by the advisor) allowed us to find the reasons for the preferences of XB and HB modes of bonding.

3.2. Structural preferences Anion-π Interactions and Halogen Bonds

According to the electrostatic model, anions are attracted to the area of most positive potential because anions have a negative charge.[5] Most aromatic complexes have their most positive area in the center of the ring due to the electrons being pulled away from the center (shown as blue in Figure 10), so it is an ideal place for an anion to make a contact.

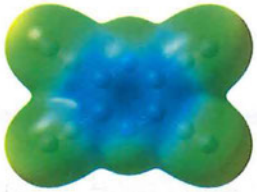

Figure 10. Electrostatic potentials on the surface of TCP showing area of positive charge (blue) over its center.

In previous work done by this research lab,[7,8] it was noted that the anions in an anion-π complexes with TCP did not line up the way the electrostatic model predicted. So, to check if these deviations were consistent and reproducible, we prepared several new crystals of similar complexes. The structure of one such complex is illustrated in Figure 11.

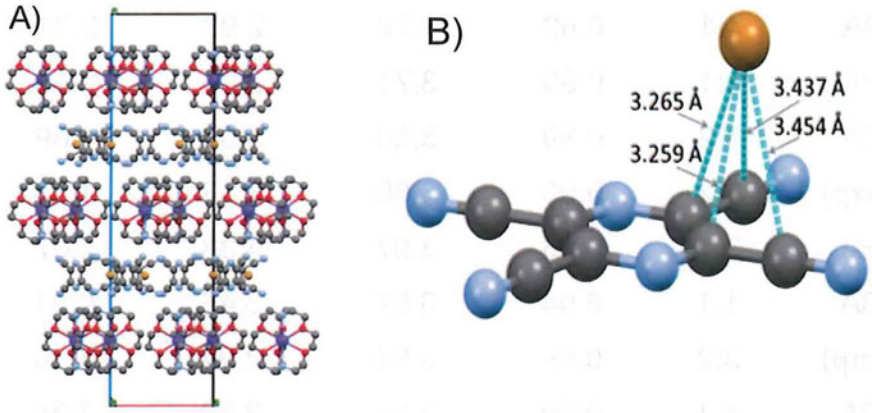

Figure 11: A) X-ray structure of K(crp)Br-TCP crystal. B) In most anion-π interactions, the anion is seen over the center of the ring. However, in this crystal the anion was found near the edge of the ring and it had shorter van der Waal radii than what is typically seen when there is an intermolecular attraction.

This complex shows very short distances between bromide anions (brown sphere) and carbons (grey spheres). This indicates strong attraction between the Br^- anions and TCP π-acceptor. Most notably, this structure shows that anion is located not

over the center, but over the edge of the TCP molecule. This same general, arrangements were observed in other crystals which were prepared and in the earlier reported X-ray structures of the TCP with halide anions.[4] It was also noted that the distances between the halides and the center of the aromatic ring (d_{cent}) were larger than the distances from the anions to the plane (d_{plane}) regardless of the anion or counter-ion as well as stoichiometry of the crystals. Accordingly, the anions are located above the edge of the TCP in all these complexes, which can be seen in Figure 11B and for all other complexes in Figure 12.

Table 3. Characteristics of TCP acceptor with halide anions (X^-) in their solid state.

X	Counter-ion	TCP:X^-	R_{XY}[a]	d_{cent}, Å[b]	d_{plane}, Å[c]	d_{off} Å[d]
Br	K^+(crp)	3:2	0.92	3.60	3.11	1.82
Br	TBA	4:1	0.89	3.72	2.99	2.21
Br	TPA	4:1	0.89	3.71	2.99	2.19
Br	TEA	3:2	0.89	3.50	3.06	1.69
I	K^+(crp)	3:2	0.93	3.60	3.33	1.38
I	TEA	2:1	0.96	3.97	3.38	2.07
I	TBA	1:1	0.94	3.57	3.45	0.91
Cl	K^+(crp)	3:2	0.89	3.61	2.94	2.10
Cl	TPA	4:1	0.89	3.65	2.88	2.24
Cl	TBA	4:1	0.89	3.66	2.88	2.26

a) Shortest X^-…C contact. The sums of the van der Waals radii for Cl···C, Br···C, and I···C contacts are 3.45 Å, 3.55 Å, and 3.68 Å respectively. b) Distance from the halogen to the center of the aromatic ring. c) Distance from the halogen to the plane of the aromatic ring. d) $d_{off} = (d_{cent}^2 - d_{plane}^2)^{05}$

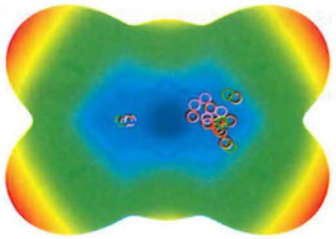

Figure 12: The electrostatic model predicts that the anions would be located over the dark blue middle due to the fact that it is the highest positive potential (π-hole). However, the actual locations of Cl^- (green), Br^- (brown), and I^- (pink) are depicted as solid lined circles.

So, the projections of the locations of the anions over the plane of TCP deviate in all cases from the locations of the most positive potential, which is at the center of TCP.

Similar deviations of the locations of the intermolecular contacts from the prediction of the electrostatic model were observed in the halogen bonded complexes of CBr_3F and CBr_4 with pseudohalide anions. The structures of the complexes which we prepared showed that these molecules approach anions from the sides.

Such tendencies are observed in other complexes – all contacts are on the side of anions (Figure 13). However, the most negative potentials (show as red areas) are located on the top of the pseudohalide anions. Obviously, there are deviations from the electrostatic models in all these cases.

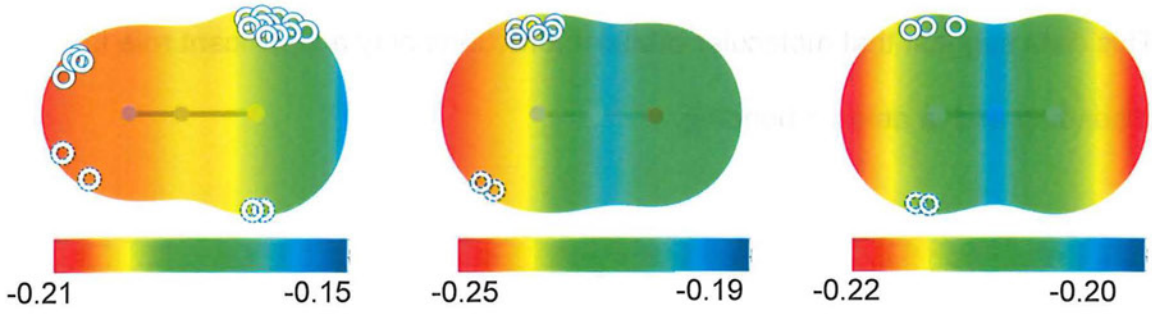

Figure 13. The locations of intermolecular contacts for the CBr_4 and CBr_3F onto the ESPs of the NCS^- (left), NCO^- (center) and N_3^- (right) anions.

To explain these deviations, we looked at the molecular orbitals of the interacting species. We found, that in all cases, locations of contacts follow the locations of molecular orbitals (Figure 14 and 15).

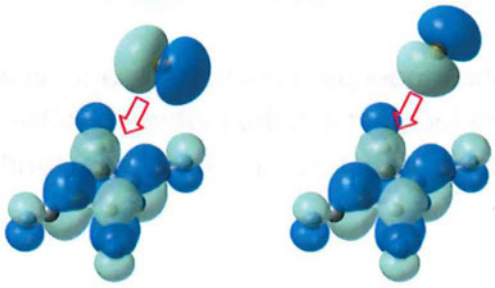

Figure 14. Molecular-orbital model of formation of TCP•X^- complexes

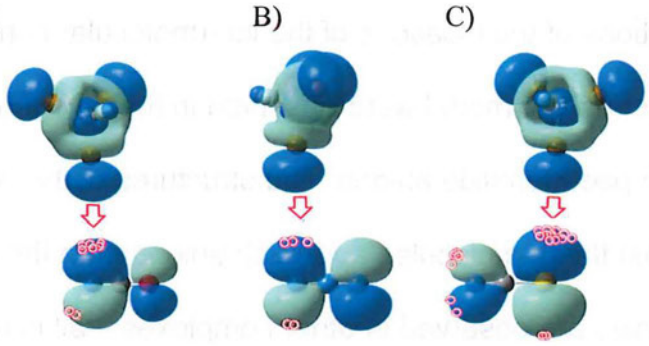

Figure 15. The frontier orbital interaction for CBr_3F with A) NCO^-, B) N_3^-, and C) NCS^-. The red circles show the intermolecular contacts.

This data suggest that molecular orbital interactions play a significant role in halogen bonding and in anion-π bonding.

Conclusions

UV-Vis, NMR and X-ray crystallographic studies showed that CHI_3 prefer halogen bonds with anions rather than hydrogen bonds. With that conclusion, spectral data showed that halogen bonds create in new absorption bends in a UV-Vis spectra as well as an upfield shift in ^{1}HNMR while hydrogen bonds result in no new absorption bends in UV-Vis and a downfield shift in a ^{1}HNMRs spectra.

X-ray structures established the anion-π complexes of TCP with halides, as well as in the complexes of CBr_4 or CBr_3F with pseudohalides had contacts that deviated from the location of the most negative or positive potentials. It was determined that the frontier-orbital shapes of these reactants indicate that structures of all of these complexes follow HOMO/LUMO interactions instead of the widely accepted electrostatic model. It shows that frontier-orbital interactions play a part in determining the structures of these intermolecular complexes.

References

1. G. Cavallo, P. Metrangolo, R. Milani, T. Pilati, A. Priimagi, G. Resnati and G. Terraneo, *Chem. Rev.,* 2016, **16**, 2478.
2. P. Politzer, J. Murray and T. Clark, *Phys.Chem. Chem. Phys.* 2010**, 12**, 7748. (b) P. Politzer, J. Murray and T. Clark, *Phys.Chem. Chem. Phys.* 2013, **15**, 11178.
3. D. Quinonero, C. Garau, C. Rotger, A. Frontera, P. Ballester, A. Costa and P. M. Deya, *Angew. Chem. Int. Ed.*, 2002, **41**, 3389.
4. Y. Rosokha, S. Lindeman, S. Rosokha and J. Kochi, *Angew. Chem., Int. Ed.,* 2004, **43**, 4650.
5. A. Bauza, T. Mooibroek and A. Frontera, *Chem. Record*, 2016, **16**, 473.
6. A. Legon, *Angew. Chem. Int. Ed* 1999, ***38***, 2686–2714.
7. S. Rosokha and A. Kumar, *J. Mol. Struct.*, 2017, **1138,** 129.
8. S. Rosokha and M. Vinakos, *Cryst. Growth Des.* 2012, **12**, 4149.